# A Comparison of Extratropical Cyclones in Recent Reanalyses ERA-Interim, NASA MERRA, NCEP CFSR, and JRA-25

K. I. HODGES, R. W. LEE, AND L. BENGTSSON

*National Centre for Earth Observation, University of Reading, Reading, United Kingdom*

(Manuscript received 24 September 2010, in final form 22 February 2011)

ABSTRACT

Extratropical cyclones are identified and compared using data from four recent reanalyses for the winter periods in both hemispheres. Results show the largest differences occur between the older lower resolution 25-yr Japanese Reanalysis (JRA-25) when compared with the newer high resolution reanalyses, particularly in the Southern Hemisphere (SH). Spatial differences between the newest reanalyses are small in both hemispheres and generally not significant except in some common regions associated with cyclogenesis close to orography. Differences in the cyclone maximum intensitites are generally related to spatial resolution except in the NASA Modern Era Retrospective-Analysis for Research and Applications (NASA MERRA), which has larger intensities for several different measures. Matching storms between reanalyses shows the number matched between the ECMWF Interim Re-Analysis (ERA-Interim) and the other reanalyses is similar in the Northern Hemisphere (NH). In the SH the number matched between JRA-25 and ERA-Interim is lower than in the NH; however, for NASA MERRA and the NCEP Climate Forecast System Reanalysis (NCEP CFSR), the number matched is similar to the NH. The mean separation of the identically same cyclones is typically less than 2° geodesic in both hemispheres for the latest reanalyses, whereas JRA-25 compared with the other reanalyses has a broader distribution in the SH, indicating greater uncertainty. The instantaneous intensity differences for matched storms shows narrow distributions for pressure, while for winds and vorticity the distributions are much broader, indicating larger uncertainty typical of smaller-scale fields. Composite cyclone diagnostics show that cyclones are very similar between the reanalyses, with differences being related to the intensities, consistent with the intensity results. Overall, results show NH cyclones correspond well between reanalyses, with a significant improvement in the SH for the latest reanalyses, indicating a convergence between reanalyses for cyclone properties.

## 1. Introduction

Reanalyses have become an important means of producing observationally constrained data for studying atmospheric circulation systems. They are produced using numerical weather prediction (NWP) systems producing analyses (initial conditions for a forecast) at subdaily frequency. This is done by combining historical atmospheric observations with a comprehensive model of the atmosphere using data assimilation to produce homogenous four-dimensional data. As NWP systems are continuously improving with the introduction of new data assimilation methods and models (Kalnay 2003), it is important to continuously redo the reanalyses to extract more information from the available observations and to provide us with better long-term data for climate studies (Bengtsson and Coauthors 2007).

Reanalyses have been popular for a wide range of studies of the atmosphere owing to their homogenous nature compared to raw observations. One of the areas where reanalyses are important is in the study of extratropical cyclones. Reanalyses are important, not only to provide information on the properties, climatology, and variability of extratropical cyclones (Hoskins and Hodges 2002, 2005), but also to provide a means of validating climate models with respect to these storms, for example, Bengtsson et al. (2006) and Bengtsson et al. (2009). However, to have confidence in such studies it is important to understand the uncertainties in the representation of cyclones in the reanalyses.

One way to explore the uncertainties is to intercompare the reanalyses. For extratropical cyclones this can be

*Corresponding author address:* Kevin Hodges, ESSC, University of Reading, 3 Earley Gate, Reading RG6 6AL, United Kingdom. E-mail: k.i.hodges@reading.ac.uk

DOI: 10.1175/2011JCLI4097.1

achieved by identifying them and their full life cycles in each reanalysis and then comparing their spatial distribution and properties. Several previous studies have performed these types of studies, including that of Hodges et al. (2003, 2004), Bromwich et al. (2007), Wang et al. (2006), Hanson et al. (2004), and Trigo (2006). These earlier studies made use of the older reanalyses, such as the Goddard Earth Observing System, version 1 (GEOS-1) (Schubert et al. 1993); the National Centers for Environmental Prediction (NCEP), National Center for Atmospheric Research (NCAR), and Department of Energy (DOE) reanalyses (Kalnay 2003); the 15-yr European Centre for Medium-Range Weather Forecasts (ECMWF) Re-Analysis (ERA-15) (Gibson et al. 1997) and the 40-yr ECMWF Reanalysis (ERA-40) (Uppala et al. 2005); and the 25-yr Japan Reanalysis (JRA-25) (Onogi et al. 2007). These relied on earlier forms of data assimilation and were also at relatively low resolution compared with the latest reanalyses.

Earlier studies have shown that in the Northern Hemisphere (NH) the older reanalyses generally compare well in terms of their spatial distribution and the number of cyclones that can be matched between reanalyses, including the mean separation distances of matched storms (Hodges et al. 2003, 2004; Wang et al. 2006). In the Southern Hemisphere (SH) larger differences were found, indicating a higher degree of uncertainty in the representation of extratropical cyclones there. This is likely related to how the available observations, which in the SH are dominated by satellite observations, are assimilated. In fact, for the older reanalyses with direct assimilation of radiances, such as ERA-40 and JRA-25, cyclones compare better in the SH but still not as well as in the NH.

The production of reanalyses is an ongoing program in several NWP centers with new reanalyses being produced as new models and data assimilation methods are introduced. It is important to continually evaluate new reanalyses to determine where improvements have been made and to highlight continuing deficiencies, particularly due to changes in the observing system and resolution. In this study three new reanalyses and one of the older reanalyses are explored for extratropical cyclone activity for the modern satellite period (1979–2009). The reanalyses studied are JRA-25 (Onogi et al. 2007), the ECMWF Interim Reanalysis (ERA-Interim) (Simmons et al. 2007), the National Aeronautics and Space Administration Modern Era Retrospective-Reanalysis for Research and Applications (NASA MERRA) (Rienecker et al. 2011), and the NCEP Coupled Forecast System Reanalysis (NCEP CFSR) (Saha et al. 2010; Saha et al. 2006).

This paper essentially repeats the original analysis of Hodges et al. (2003, 2004) with these more recent reanalyses. The scientific aims of the paper are twofold: first, to determine how well the new reanalyses intercompare with respect to cyclones and, hence, indicate the degree of uncertainty in their properties and, second, to see if there any improvements over the older reanalyses. The focus is on synoptic scale cyclones in both hemispheres for the winter periods. Smaller scale systems, such as mesocyclones, are likely to be more sensitive to available observations as well as the model and data assimilation.

The paper continues in section 2 with a brief description of the data and methodology used. Section 3 presents results of the spatial differences of cyclone densities, frequency distributions of cyclone intensities, and results of the direct matching between cyclones between different reanalyses, including composites. Finally, a summary and conclusions are given in section 4.

## 2. Data and methodology

The four reanalyses explored for extratropical cyclones are JRA-25, ERA-Interim, NASA MERRA, and NCEP CFSR. The JRA-25, NASA MERRA, and NCEP CFSR start in 1979 and have a similar length (1979–2009), whereas ERA-Interim begins in 1989 (1989–2009). While all four reanalyses produce analyses every 6 h, the NCEP CFSR actually has data available hourly. However, this is achieved by placing forecasts, which are available hourly, in between the analyses. In this study, only the 6-h analyses are used to be consistent with the other reanalyses.

A brief summary of each reanalysis follows with a focus on the components of the different systems that may impact the representation of extratropical cyclones.

(i) JRA-25 (Onogi et al. 2007) uses a spectral model integrated at a T106 (125 km) horizontal resolution with 40 hybrid sigma-pressure vertical levels. The prognostic equations are solved in Eulerian form (semi-Lagrangian after 2005) with finite differences in the vertical. The data assimilation is three-dimensional variational (3DVAR) data assimilation with 6-h cycling. A full range of observations are assimilated following quality control and bias correction, including satellite radiances from the Television and Infrared Observation Satellite Operational Vertical Sounder (TOVS)/Advanced TOVS (ATOVS) and precipitable water from the Special Sensor Microwave Imager (SSM/I).

(ii) ERA-Interim (Simmons et al. 2007) also uses a spectral model (Integrated Forecast System, cycle 31R1) integrated at a T255 (80 km) horizontal resolution with 60 vertical hydrid levels. The prognostic

equations are solved using the semi-Lagrangian method with a finite element method in the vertical. A four-dimensional variational (4DVAR) data assimilation system with 12-h cycling (Thépaut et al. 1993) is used with output every 6 h. Flow-dependent structure functions are used, which have the potential to extract more information from the observations, thereby improving the quality of the analyses. A new humidity analysis (Hólm et al. 2002) has reduced the problems found in ERA-40 with the assimilation of humidity observations from satellites (Bengtsson et al. 2004). A full range of observations are bias corrected before assimilation, in particular, a variational scheme is used for satellite radiances.

(iii) The NASA MERRA reanalysis (Rienecker et al. 2011) uses the GEOS, version 5 (GEOS-5) model and data assimilation system (Rienecker and Coauthors 2008). This has a finite volume model, integrated at a resolution of ⅔° longitude by ½° latitude (~55 km) with 72 Lagrangian vertical levels (Lin 2004). The data assimilation used is the gridpoint statistical interpolation (GSI) system originally developed by NCEP (Wu et al. 2002) with 6-h cycling. This is a 3DVar system formulated in physical space to enable the implementation of flow-dependent anisotropic, inhomogeneous background error covariances (Purser et al. 2003a,b). As with all the reanalyses, observations are quality controlled and bias corrected before assimilation, including the satellite radiances. Additionally rain rates from SSM/I and the Tropical Rainfall Measuring Mission (TRMM) satellites are assimilated.

(iv) The NCEP CFSR (Saha et al. 2010) uses the NCEP Coupled Forecast System model. This consists of a spectral atmospheric model (Saha et al. 2006) at a resolution of T382 (38 km) with 64 hybrid vertical levels and the Geophysical Fluid Dynamics Laboratory (GFDL) Modular Ocean Model, version 4p0d (Griffies et al. 2004), which is a finite-difference model at a resolution of ~½° with 40 levels in the vertical. The atmosphere and ocean models are coupled with no flux adjustment. The NCEP CFSR uses the GSI data assimilation system for the atmosphere. Flow dependence for the background error variances is included as well as first-order time interpolation to the observation (FOTO) (Rančić et al. 2008). Variational quality control of observations (Andersson and Järvinen 1999) is also included. An ocean analysis for SST is also performed using optimal interpolation (OI). A full range of observations is used as in the other reanalyses, which are quality controlled and bias corrected, including satellite radiances. Observations of ocean temperature and salinity are also used.

The analysis methodology used in this study has been used in several previous studies of extratropical cyclones (e.g., Bengtsson et al. 2009, 2006; Hodges et al. 2003, 2004; Hoskins and Hodges 2002, 2005) and is based on the tracking scheme developed by Hodges (1994, 1995, 1999). Cyclones are identified as maxima or minima by the tracking scheme depending on the field chosen for the identification. In this study both mean sea level pressure (MSLP) and 850-hPa relative vorticity ($\xi_{850}$) at 6-h frequency are used to provide the traditional MSLP perspective as well as the vorticity perspective. As part of the identification, the large-scale background is first removed, as discussed in Hoskins and Hodges (2002) and Anderson et al. (2003). The resolution is also decreased to reduce noise in the identification process; this is more important for vorticity, which is a very noisy field at high resolution, than for MSLP, which is generally smoother. In this study a T63 resolution for MSLP and T42 for vorticity are used. Even though a higher resolution is used for MSLP than for vorticity, in general more cyclones are identified for vorticity than for MSLP with the chosen characteristics of lifetime and displacement distances. The fact that each reanalysis is reduced to the same resolution, for each field, for the identification means that identification is performed at the same spatial scale, which in this case focuses on the synoptic scales. The $\xi_{850}$ is the preferred field for reasons discussed in the previously mentioned studies, namely, a weaker influence of the large-scale background than is the case for MSLP, less extrapolation below orography, and the focus on smaller spatial scales.

Before analyzing the tracks, they are filtered to retain only those storms that last at least 2 days and travel farther than 1000 km so that the emphasis is on mobile cyclones. Since ERA-Interim data is available for the shortest period, this is chosen as the base reanalysis for the comparison with the other reanalyses. The main focus will be on the winter period in both hemispheres, December–February (DJF) in the NH and June–August (JJA) in the SH. Also, since the interest here is on extratropical cyclones, any storms that have the major part of their life cycle within the tropics are excluded, where the tropics are defined as the zonal region (30°S, 30°N).

Spatial statistics are computed from the cyclone tracks for each reanalysis using the spherical kernel approach (Hodges 1996). Selected spatial statistics—namely, the track and genesis densities—are differenced to highlight where differences in the distribution of cyclones between the reanalyses occur. These differences are tested

using a Monte Carlo significance test (Hodges 2008). In addition, the cyclone tracks will be referenced back to the full resolution fields of MSLP, 925-hPa winds, and $\xi_{850}$. The 925-hPa winds are used as opposed to the 10-m winds because they represent the wind field above the surface boundary layer and are specifically calculated by the model. The full resolution intensities are used to construct maximum intensity distributions to compare between the reanalyses. A more direct comparison between the cyclone tracks from the different reanalyses is also performed by matching the identically same storms between the reanalyses in the same way as in Hodges et al. (2003, 2004). The identically same storms are identified by finding the tracks with minimum mean separation distance that is less than some prescribed value, chosen here to be 4° (geodesic), and overlaps in time by at least 50% of their points. From the tracks that match, maximum intensity distributions are derived; this is also done for the tracks that do not match. From the matched tracks, statistics for the mean separation distances and instantaneous intensity differences are computed. For the storms that match, a selected number of extreme storms are used to explore and compare their life cycles and structure based on compositing, as described and used in Bengtsson et al. (2009) and Catto et al. (2010).

## 3. Results

### *a. Climatology*

Before presenting the results comparing the cyclones in the different reanalyses, the climatology of cyclones are shown for the ERA-Interim reanalysis, to provide a frame of reference.

The track and genesis densities for the NH and SH winters for $\xi_{850}$ are shown in Fig. 1. This shows cyclone distributions very similar to that obtained from older reanalyses based on the same field (Bengtsson et al. 2006; Hoskins and Hodges 2002, 2005). In particular, in the NH the two main oceanic storm tracks are well defined by high values of track density, as is the Mediterranean storm track, extending through the Middle East, and the Siberian storm track. The NH cyclogenesis (Fig. 1b) shows the well-known active regions in the lee of the Rockies, the Tibetan Plateau and the Alps (Gulf of Lyon), and over the main baroclinic regions off Cape Hatteras and east of Japan (Kuroshio region). Other more extended secondary cyclogenesis regions are also apparent in the Atlantic and Pacific Oceans. These features have been well documented in previous studies, for example, Hoskins and Hodges (2002).

In the SH (Fig. 1c), the main oceanic storm track is seen extending from South America and spiraling into the Antarctic coast, then extending to the Antarctic Peninsula. The weaker Pacific storm track extending from Australia can also be seen. The main cyclogenesis in the SH (Fig. 1d) occurs in the lee of the Andes with two centers, the poleward center associated with where the Pacific storm track meets the Andes and the equatorward center associated with where the subtropical jet crosses the Andes (this pattern is similar to that seen in the lee of the Rockies). Another major center is seen on the Antarctic coast associated with the decay and cyclolysis of cyclones spiraling into the coast from higher latitudes; these bring warm, moist air that, combined with the flow of cold air from the continent, results in enhanced local baroclinicity and reinvigoration of storms or development of new storms. Other regions are also apparent in the oceanic storm tracks associated with secondary cyclogenesis and downstream development (Chang 1993; Hoskins and Hodges 2005). These cyclone distribution features in the SH have also been documented in previous studies, for example, Hoskins and Hodges (2005). If MSLP is used to identify cyclones (not shown), the distributions are in general very similar albeit with lower density values due to the lower number of identified cyclones.

The results that follow comparing the reanalysis from the perspective of extratropical cyclone properties are presented as several different types of diagnostics, starting with numbers and spatial statistics. This is followed by distributions of maximum intensities for different measures of intensity, determined at full native resolution. Next, to explore which storms are common to the reanalyses and to perform a more direct comparison of intensities, results are shown based on cyclone matching. Finally results will be shown comparing the composite cyclones.

### *b. Numbers and difference in spatial distribution*

The number of cyclones identified shows fewer storms are identified in JRA-25 than in either of the other three reanalyses and that ERA-Interim and NCEP CFSR, in general, have the most storms for both MSLP and $\xi_{850}$ in both hemispheres. More cyclones are identified using the $\xi_{850}$ field than the MSLP field, with the chosen lifetime and displacement properties, for all seasons. This is the case even though the identification is performed at a lower resolution for $\xi_{850}$. In fact, if the MSLP is used at an even higher resolution, this would still be the case (Froude 2010). In general, the differences in numbers between the reanalyses are relatively small: a summary is given in Table 1. Larger differences are expected when focusing on smaller-scale mesocyclones.

To explore the differences and similarities between the cyclone spatial distributions, the differences of track

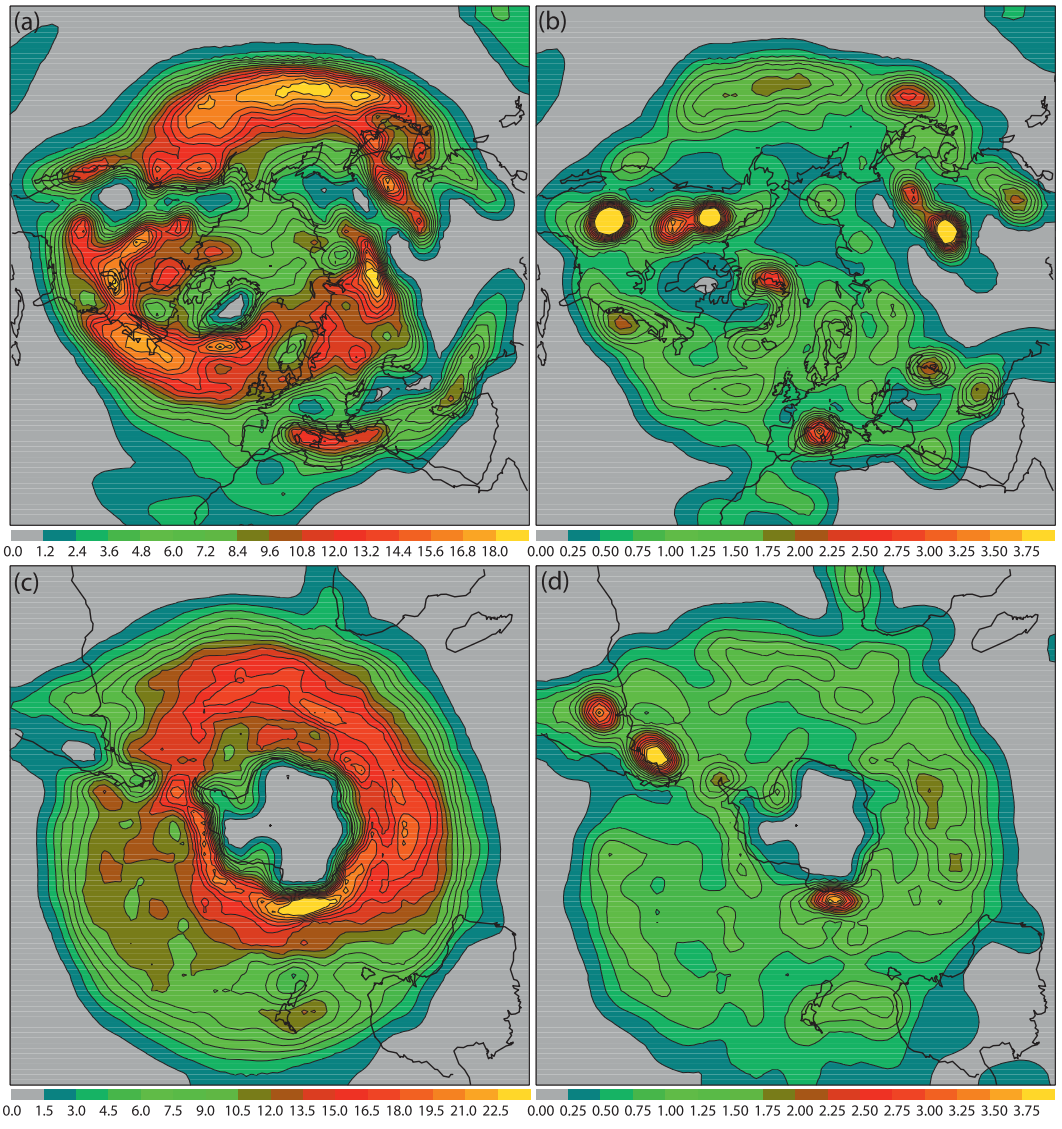


FIG. 1. Extratropical cyclone climatology based on the ERA-Interim reanalysis (1989–2009), $\xi_{850}$, (a) NH, DJF track density; (b) NH, DJF genesis density; (c) SH, JJA track density; and (d) SH, JJA genesis density. Densities are in units of number density per month per unit area, where the unit area is equivalent to a 5° spherical cap ($\sim 10^6$ km$^2$).

and genesis densities are determined between ERA-Interim and the other reanalyses for $\xi_{850}$ for the NH and SH winters. Results for MSLP (not shown) indicate similar results. The regions where the distributions are statistically different are indicated where the $p$ values (Hodges 2008) for the differences are below 0.05 (significance level of 95%). From the ''frequentist'' view point, this is where the hypothesis should be rejected, that the two distributions (from which the differences are computed) are drawn from the same underlying distribution.

The results for the comparison in the NH winter are shown in Fig. 2. For the ERA-Interim comparison with JRA-25 the track density shows relatively small differences (Fig. 2a), which are not statistically significant at the 95% level. There are some regions that show larger differences, which are significant, with the largest of these seen at the end of the Mediterranean storm track. This is a similar result to that seen in the older reanalysis (Hodges et al. 2003) and associated with weak systems that are sensitive to the observations and their assimilation. For the genesis differences (Fig. 2b), there are relatively large differences, which are significant, associated with the orographic regions in the lee of the Rockies and the Himalayan massif as well as at the end of the Mediterranean storm track. This may be expected owing to the different representation of the orography and orographic processes

TABLE 1. Number of cyclones per month for each season, field, and reanalysis that are found in the NH and SH extratropics, (30°, 90° N/S) for the period 1989–2009.

| | | Season | | | | | | | |
|---|---|---|---|---|---|---|---|---|---|
| | | DJF | | MAM | | JJA | | SON | |
| | | NH | SH | NH | SH | NH | SH | NH | SH |
| JRA-25 | MSLP | 77.2 | 60.8 | 77.7 | 68.9 | 65.5 | 69.3 | 73.2 | 62.9 |
| | $\xi_{850}$ | 123.2 | 98.0 | 118.1 | 111.6 | 96.5 | 122.3 | 109.6 | 112.9 |
| NASA MERRA | MSLP | 78.5 | 65.1 | 82.0 | 76.0 | 70.2 | 79.4 | 75.0 | 75.9 |
| | $\xi_{850}$ | 124.5 | 101.4 | 117.0 | 117.0 | 97.2 | 125.4 | 109.3 | 118.0 |
| NCEP CFSR | MSLP | 77.8 | 68.1 | 79.7 | 76.3 | 67.5 | 80.1 | 74.7 | 75.8 |
| | $\xi_{850}$ | 128.5 | 106.1 | 120.7 | 123.0 | 101.0 | 130.6 | 113.5 | 122.7 |
| ERA-Interim | MSLP | 80.8 | 66.9 | 81.3 | 77.5 | 67.9 | 82.1 | 75.0 | 78.7 |
| | $\xi_{850}$ | 130.8 | 104.1 | 121.5 | 120.9 | 100.0 | 130.9 | 112.5 | 121.0 |

at the two different resolutions of the ERA-Interim and JRA-25.

For the differences between ERA-Interim and NASA MERRA in the NH (Figs. 2c,d) it is apparent that, in general, the differences are smaller than those between ERA-Interim and JRA-25. This might be expected as the resolutions are more similar between ERA-Interim and NASA MERRA. The differences in track density (Fig. 3c) are similar to those seen in the JRA-25 comparison with the largest significant region of differences at the end of the Mediterranean storm track. For the cyclogenesis (Fig. 3d) there is an obvious improvement in the agreement in the lee of the Rocky Mountains, with much smaller differences compared with the JRA-25 comparison. This is likely due to the representation of the orography being similar at the more similar resolutions of ERA-Interim and NASA MERRA. The difference in the genesis in the Middle East is also smaller in this comparison though still large enough to be significant at the 95% level. The largest difference in genesis occurs on the eastern side of the Himalayas, though it shows some improvement over the JRA-25 comparison, particularly the southern Mongolian genesis. The reason why this difference persists even between reanalyses of similar resolution is unclear. The Altai Mountains in this region are relatively high, reaching up to 6000 m; however, the differences may be due to these systems being relatively weak and more sensitive to the model, observations, and data assimilation—similar to the Middle Eastern region.

The differences between ERA-Interim and NCEP CFSR in the NH are shown in Figs. 2e and 2f. These show the smallest differences compared to the comparisons with NASA MERRA and JRA-25. The track density differences (Fig. 2e) are almost zero in the main oceanic storm tracks, and even at the end of the Mediterranean storm track through the Middle East the differences are much reduced though still significant. The differences in the cyclogenesis (Fig. 2f) are also smallest of all of the comparisons, particularly in the lee of the Rockies. However, the Mongolian region still stands out as a region with significant differences in genesis.

The difference statistics for the SH winter are shown in Fig. 3. For the difference in track density between ERA-Interim and JRA-25 (Fig. 3a) larger differences can be seen than was the case in the NH winter, particularly through the Atlantic and Indian Ocean sectors with large regions having $p$ values below 0.05%. The genesis also shows large differences (Fig. 3b), again, in association with the orography, particularly in the lee of the Andes, similar to that seen in the NH in the lee of the Rockies. In comparison with previous studies with the older reanalyses (Hodges et al. 2003, 2004; Wang et al. 2006), these results do not show any major changes or improvements in agreement in the SH. For the difference between NASA MERRA and ERA-Interim the track density (Fig. 3c) shows more obviously smaller differences than for the JRA-25 comparison, with smaller and fewer regions that are significant. For the cyclogenesis (Fig. 3d) the differences are similar to those shown for the JRA-25 comparison; in particular, the lee of the Andes still shows relatively high and significant difference values, with ERA-Interim showing higher levels of genesis. This may be partly due to the narrow and sharp Andes being more difficult to represent compared to, say, the broader Rocky Mountains in the NH, even at the resolutions of ERA-Interim and NASA MERRA. The track density differences between NCEP CFSR and ERA-Interim (Fig. 3e) are small and comparable with those in the NH and much less than for the other two comparisons. The differences in cyclogenesis (Fig. 3f) also show the smallest differences compared with the other two comparisons, including in the lee of the Andes.

These spatial comparisons highlight a general convergence between the newer high-resolution reanalyses in terms of cyclone numbers and distribution. This is

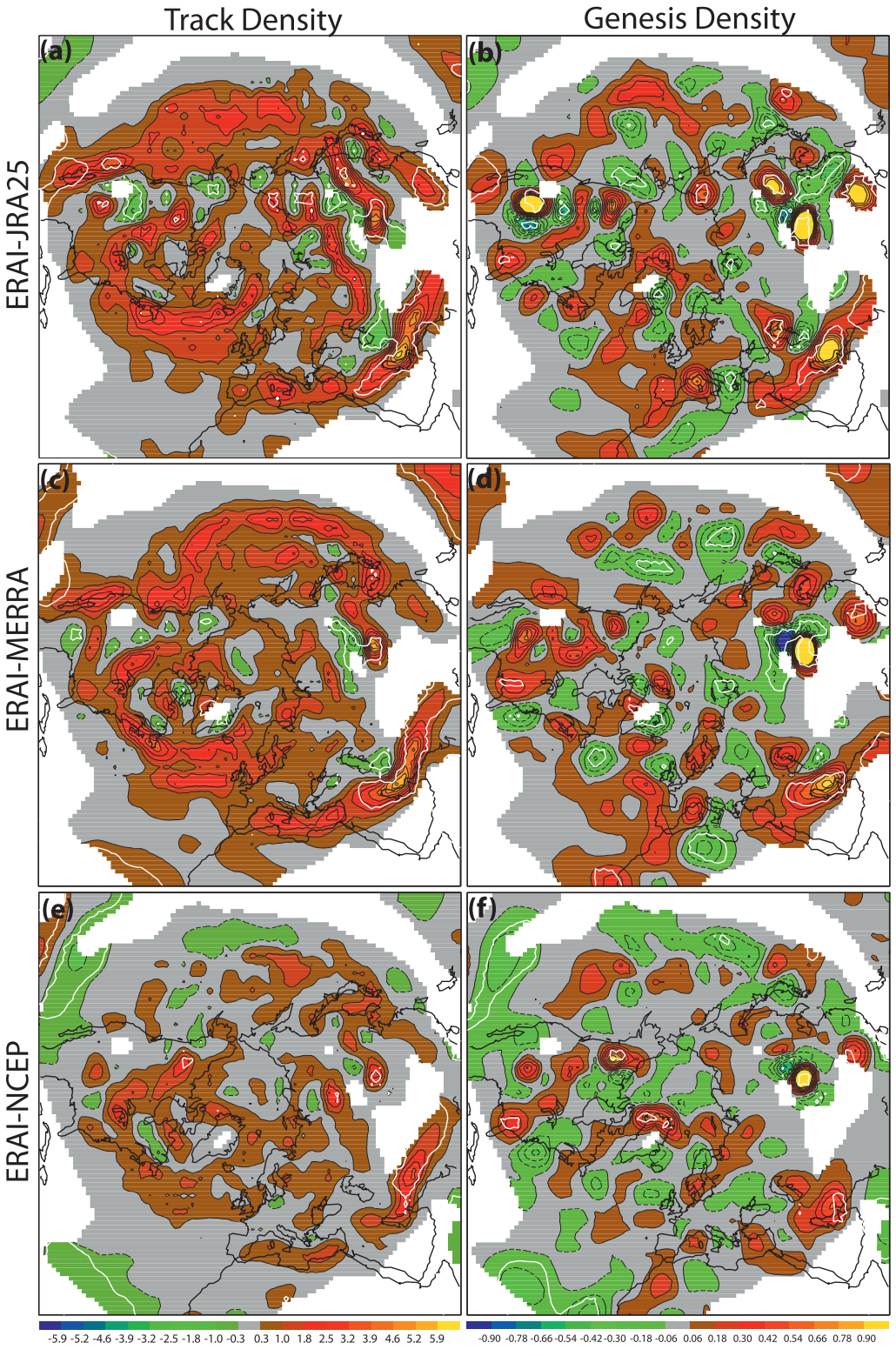


FIG. 2. Difference in $\xi_{850}$ extratropical cyclone track and genesis densities between ERA-Interim, JRA-25, NASA MERRA, and NCEP CFSR for the NH in DJF for the period 1989–2009: (left) track density differences (a) ERA-Interim − JRA-25, (c) ERA-Interim − MERRA, and (e) ERA-Interim − NCEP and (right) genesis density differences (b) ERA-Interim − JRA-25, (d) ERA-Interim − MERRA, and (f) ERA-Interim − NCEP. The white lines delineate regions where $p$ values for the differences are below 0.05. Densities are in units of number density per month per unit area, where the unit area is equivalent to a 5° spherical cap ($\sim 10^6$ km$^2$).

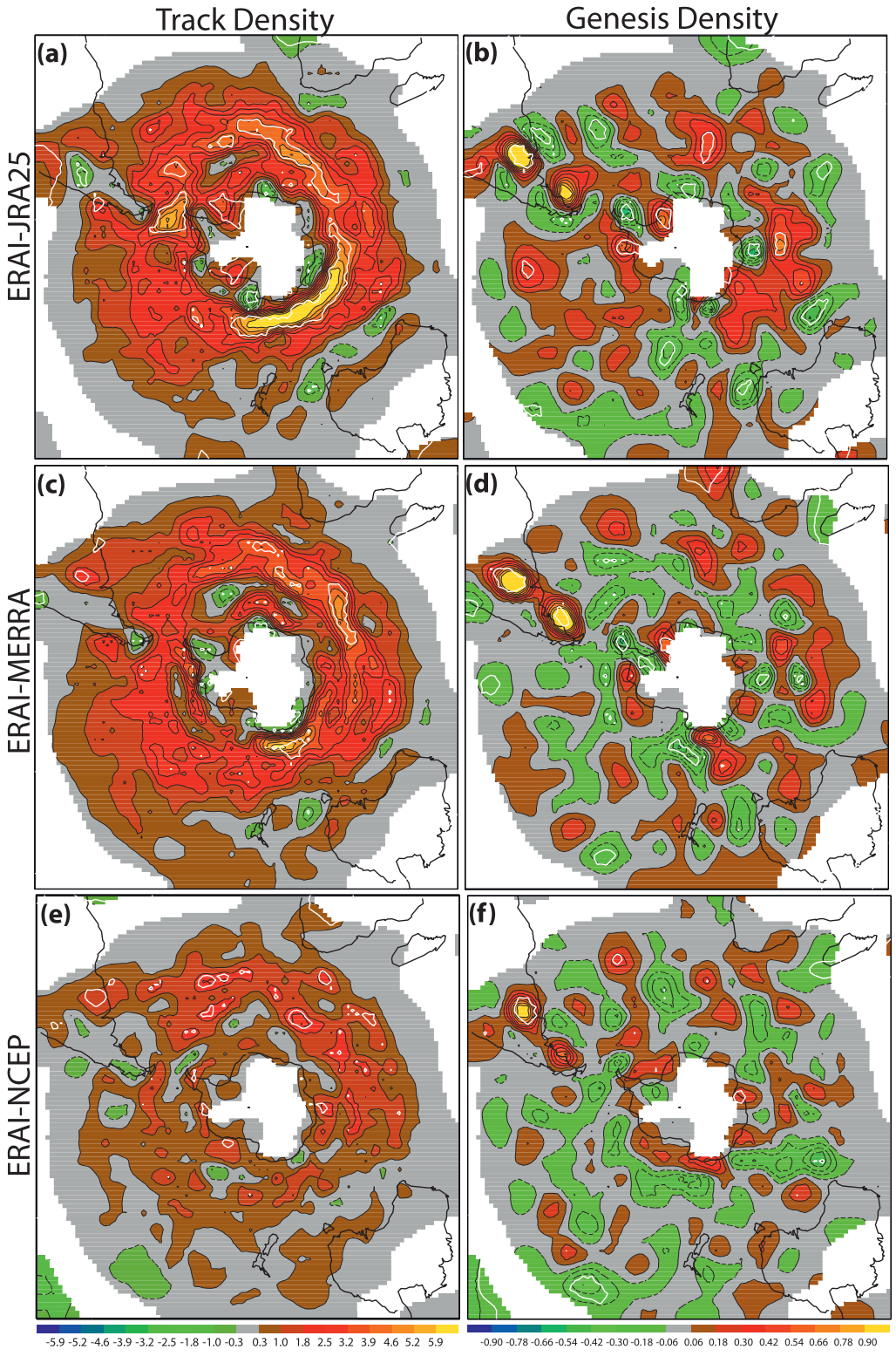


FIG. 3. As in Fig. 2 but for the SH in JJA.

particularly the case in the SH, which shows a significant improvement between the newer higher resolution reanalyses compared to the older reanalyses. The ERA-Interim comparison with NCEP CFSR in the SH is as good as in the NH. This likely reflects the general improvement in the data assimilation and forecast models, in particular the use of satellite observations, which has resulted in a significant improvement in recent years in forecast skill in the SH to a level that it is comparable to the NH (Thépaut and Andersson 2003).

### c. Intensity distributions

The maximum intensity distributions of the cyclones referenced to full resolution for MSLP, 925-hPa winds, and $\xi_{850}$ fields are determined as described in Bengtsson et al. (2009). Values are determined within a prescribed radius of the cyclone center. The radius is taken as 5.0° (geodesic) for MSLP and vorticity and 6.0° for winds. The maximum attained intensity is obtained for all tracks, excluding those in the tropics.

The distributions for MSLP referenced to the MSLP tracks provide the more traditional perspective and are shown in Figs. 4a and 4b for the NH and SH winters, respectively; the insets show the extreme tails scaled to 90 months. For the NH winter, Fig. 4a shows that the distributions for the four reanalyses appear to be very similar, with a skewed distribution. However, it is apparent that NASA MERRA has deeper extreme systems than the other three reanalyses and JRA-25 has the weakest extremes. For the SH winter, shown in Fig. 4b, the distributions are also very similar but are more heavily skewed to deeper systems associated with the circumpolar pressure trough. Similar to the NH, NASA MERRA has the deeper extreme systems and JRA-25 the weakest systems; this appears more apparent in the SH. As the distributions are very similar, a two-sided Kolmogorov–Smirnov test is performed to test when and if they are statistically different. This is a nonparametric method; these tend to have less statistical power than parametric methods, but do not depend on any distributional assumptions. Table 2 shows the Kolmogorov–Smirnov statistic $D$ (the maximum distance between the cumulative distributions) and the associated $p$ values. The distributions are considered statistically different if $p < 0.05$, that is, significant at the 95% level; this occurs for relatively high values of $D$. Table 2 shows that in the NH winter the NASA MERRA distribution is statistically different from those of the other reanalyses. For the SH winter NASA MERRA is also statistically different from the other reanalyses, as is JRA-25. The other seasons are also shown in Table 2 for completeness and show that NASA MERRA and JRA-25 are statistically different for other seasons as well.

For the 925-hPa winds referenced to the $\xi_{850}$ tracks, the maximum intensity distributions are shown in Figs. 4c and 4d for the NH and SH winters, respectively. These show much larger differences between the reanalyses than was the case for MSLP. In the NH (Fig. 4c) it is apparent that NASA MERRA still has the more extreme cyclones, followed by NCEP CFSR, and then ERA-Interim, and the weakest extremes are found in JRA-25. In many ways these results are not too surprising for NCEP CFSR, ERA-Interim, and JRA-25 with the intensities following the resolution. The fact that NASA MERRA shows more extreme cyclones than the other reanalyses, even though it is not the highest resolution reanalysis, is perhaps more surprising but is a likely consequence of the deeper systems in NASA MERRA. In the SH (Fig. 4d) a similar picture is seen, although the distributions are perhaps even more different with different shapes. NASA MERRA still has the strongest extremes, while ERA-Interim has a narrower distribution and NCEP CFSR has a broader distribution.

The maximum (minimum) vorticity distributions for the vorticity tracks referenced to full resolution for the NH (SH) winter periods are shown in Fig. 4e and 4f). Note that in the SH values are multiplied by $-1$. Vorticity is more sensitive for measuring intensity as geostrophically it depends on second-order derivatives. The results for this field show that intensities are as would be expected, with the maximum intensities being highest in the highest resolution reanalysis of NCEP CFSR and lowest in the lowest resolution reanalysis of JRA-25 for winters in both hemispheres. This is different from the results for winds and pressure and indicates that the resolution is the more important factor in determining the small-scale structure. The distributions for both winds and vorticity are so obviously different between the reanalyses that no significance test was performed.

### d. Track matching

Since the reanalyses will in general assimilate the same observations over the same period, they should simulate the identically same storms. This makes it possible to also compare the same storms between reanalyses (Bromwich et al. 2007; Hodges et al. 2003, 2004; Wang et al. 2006). This allows a more detailed comparison of the cyclones between the different reanalyses to be performed. This is achieved using a track matching algorithm (Hodges et al. 2003, 2004), as described in section 2, and constructing statistics based on these matches.

Results for the number of matches for each pair of reanalyses and for both MSLP and $\xi_{850}$ are shown in Table 3. This shows that, in the NH winter and using the ERA-Interim as the base reanalysis, the largest number of matches occur for NCEP CFSR for both MSLP (81%)

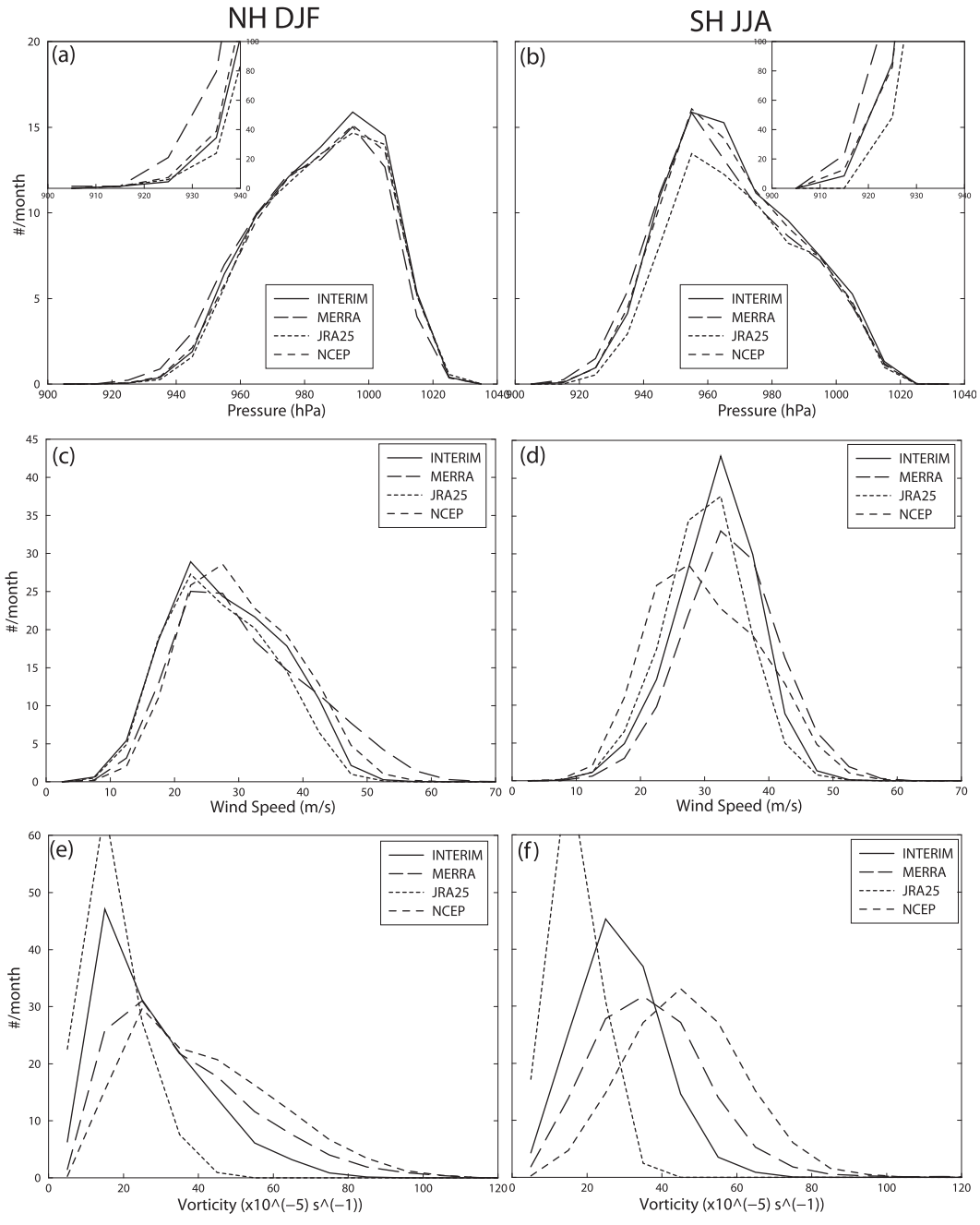


FIG. 4. Maximum intensity distributions based on full-resolution MSLP, 925-hPa winds, and $\xi_{850}$ for the winter periods in the (left) NH (DJF) and (right) SH (JJA): MSLP referenced to MSLP tracks (a) in the NH for DJF and (b) in the SH for JJA; 925-hPa winds referenced to $\xi_{850}$ tracks (c) in the NH for DJF and (d) in the SH for JJA; and $\xi_{850}$ referenced to $\xi_{850}$ tracks (e) in the NH for DJF and (f) in the SH for JJA. Values are number per month for the period 1989–2009. Bin widths are 10 hPa for MSLP, 5 m $s^{-1}$ for winds, and $10 \times 10^{-5}$ $s^{-1}$ for vorticity; SH vorticity is scaled by $-1$.

and $\xi_{850}$ (81%), with a lower number for NASA MERRA (79%, 76%) and JRA-25 (80%, 76%). For the 10% most intense systems in ERA-Interim, the number of matches rises to 97% for $\xi_{850}$. For the SH winter (JJA), again using ERA-Interim as the base reanalysis, the comparison with NASA MERRA (81%, 75%) and NCEP CFSR (84%, 81%) shows a similar number of matches per month, comparable to those in the NH winter, while for the comparison with JRA-25 (67%, 66%), there is a much lower number of matches. To see which types of systems

TABLE 2. Kolmogorov–Smirnov statistic ($D$) and associated $p$ value for the comparison of the MSLP intensity distributions in the NH and SH for the respective seasoms. Bold values in the table indicate $p$ values below 0.05, i.e., significant at 95%.

| | | Season | | | | | | | |
|---|---|---|---|---|---|---|---|---|---|
| | | DJF | | MAM | | JJA | | SON | |
| | | NH | SH | NH | SH | NH | SH | NH | SH |
| ERA-Interim – NCEP | $D$ | 0.0143 | 0.0151 | 0.0105 | 0.0157 | 0.0266 | 0.0123 | 0.0165 | 0.0135 |
| | $p$ | 0.7273 | 0.7573 | 0.9448 | 0.5998 | 0.0988 | 0.8406 | 0.5503 | 0.7807 |
| ERA-Interim – MERRA | $D$ | 0.0463 | 0.0181 | 0.0416 | 0.0308 | 0.0416 | 0.0419 | 0.0423 | 0.0235 |
| | $p$ | **0.0000** | 0.5446 | **0.0002** | **0.0219** | **0.0011** | **0.0003** | **0.0004** | 0.1484 |
| ERA-Interim – JRA-25 | $D$ | 0.0184 | 0.0546 | 0.0202 | 0.0389 | 0.0223 | 0.0377 | 0.0235 | 0.0280 |
| | $p$ | 0.4152 | **0.0000** | 0.2613 | **0.0023** | 0.2494 | **0.0028** | 0.1551 | 0.0737 |
| MERRA–NCEP | $D$ | 0.0379 | 0.0197 | 0.0430 | 0.0222 | 0.0581 | 0.0386 | 0.0423 | 0.0165 |
| | $p$ | **0.0026** | 0.4326 | **0.0002** | 0.1963 | **0.0000** | **0.0013** | **0.0005** | 0.5485 |
| MERRA–JRA-25 | $D$ | 0.0502 | 0.0545 | 0.0321 | 0.0625 | 0.0400 | 0.0713 | 0.0469 | 0.0390 |
| | $p$ | **0.0000** | **0.0000** | **0.0114** | **0.0000** | **0.0022** | **0.0000** | **0.0000** | **0.0036** |
| NCEP–JRA-25 | $D$ | 0.0142 | 0.0517 | 0.0262 | 0.0455 | 0.0461 | 0.0402 | 0.0212 | 0.0292 |
| | $p$ | 0.7516 | **0.0000** | 0.0678 | **0.0002** | **0.0003** | **0.0012** | 0.2517 | 0.0574 |

match and do not match, the maximum intensities of each system are used to determine the distribution for the matching and nonmatching systems; this is done based on the T42, $\xi_{850}$ intensities. Figure 5 shows that in the NH the storms that match cover a broad range of intensities for each comparison, while those storms that do not match tend to be the weaker storms. This is true for each of the comparisons in the NH. The best comparison occurs for the ERA-Interim matched against NCEP CFSR. In the SH it is apparent that, as well as having a lower proportion of matches, JRA-25 has a broader distribution of intensities for the storms that do not match. This was also found to be the case with the older reanalyses (Bromwich et al. 2007). For the newer reanalyses there is a significant improvement in the SH in terms of the matched storms compared with the older reanalyses.

This comparison can be extended further to look at the differences in more detail for the matched tracks by computing the distributions of mean separation distances and the instantaneous intensity differences for all pairs of points that match. The distribution of mean separation distances for the storms that match are shown in Fig. 6 as a probability density function (PDF) distribution for the NH and SH winters. For the NH winter Fig. 6a shows that the results are similar to those obtained for the older reanalyses (Hodges et al. 2004; Wang et al. 2006); namely, the matched storms do so predominantly for mean separation distances less than 2.0° (geodesic). However, there is a significant improvement over the older reanalyses with the majority of matches now occurring for mean separation distances less than 1.0° and with more similar distributions between the different reanalyses. The best matches occur between ERA-Interim and NCEP CFSR with a distribution shifted to smaller mean separation distances. In the SH, Fig. 6b shows that the comparison for the matches

TABLE 3. Number of storms per month that match between the reanalyses for the 1989–2009 period and for the different seasons for both MSLP and $\xi_{850}$ in both NH and SH excluding the tropics.

| | | Season | | | | | | | |
|---|---|---|---|---|---|---|---|---|---|
| | | DJF | | MAM | | JJA | | SON | |
| | | NH | SH | NH | SH | NH | SH | NH | SH |
| Interim – MERRA | MSLP | 64.1 | 54.2 | 66.1 | 62.8 | 53.2 | 66.8 | 61.5 | 63.2 |
| | $\xi_{850}$ | 99.8 | 77.6 | 94.3 | 90.0 | 76.3 | 98.3 | 87.9 | 91.1 |
| Interim – JRA-25 | MSLP | 64.8 | 48.8 | 64.8 | 55.8 | 51.7 | 55.0 | 61.4 | 49.6 |
| | $\xi_{850}$ | 99.5 | 71.2 | 95.3 | 81.3 | 75.8 | 87.1 | 89.1 | 80.6 |
| Interim – NCEP | MSLP | 65.7 | 56.0 | 67.4 | 64.6 | 55.1 | 68.8 | 63.3 | 64.9 |
| | $\xi_{850}$ | 106.7 | 84.6 | 98.8 | 96.9 | 80.8 | 106.5 | 92.8 | 97.2 |
| MERRA – JRA-25 | MSLP | 62.2 | 47.7 | 63.3 | 53.8 | 51.3 | 52.8 | 59.3 | 47.7 |
| | $\xi_{850}$ | 94.1 | 67.8 | 90.4 | 77.5 | 73.7 | 83.1 | 85.5 | 77.5 |
| MERRA – NCEP | MSLP | 63.1 | 53.5 | 64.7 | 61.4 | 52.7 | 65.4 | 60.9 | 60.9 |
| | $\xi_{850}$ | 99.4 | 77.5 | 92.7 | 89.6 | 76.6 | 97.4 | 87.8 | 91.1 |
| NCEP – JRA-25 | MSLP | 63.7 | 48.2 | 63.7 | 54.8 | 51.3 | 53.7 | 60.6 | 47.3 |
| | $\xi_{850}$ | 97.9 | 69.8 | 93.4 | 79.9 | 75.6 | 85.1 | 88.0 | 80.2 |

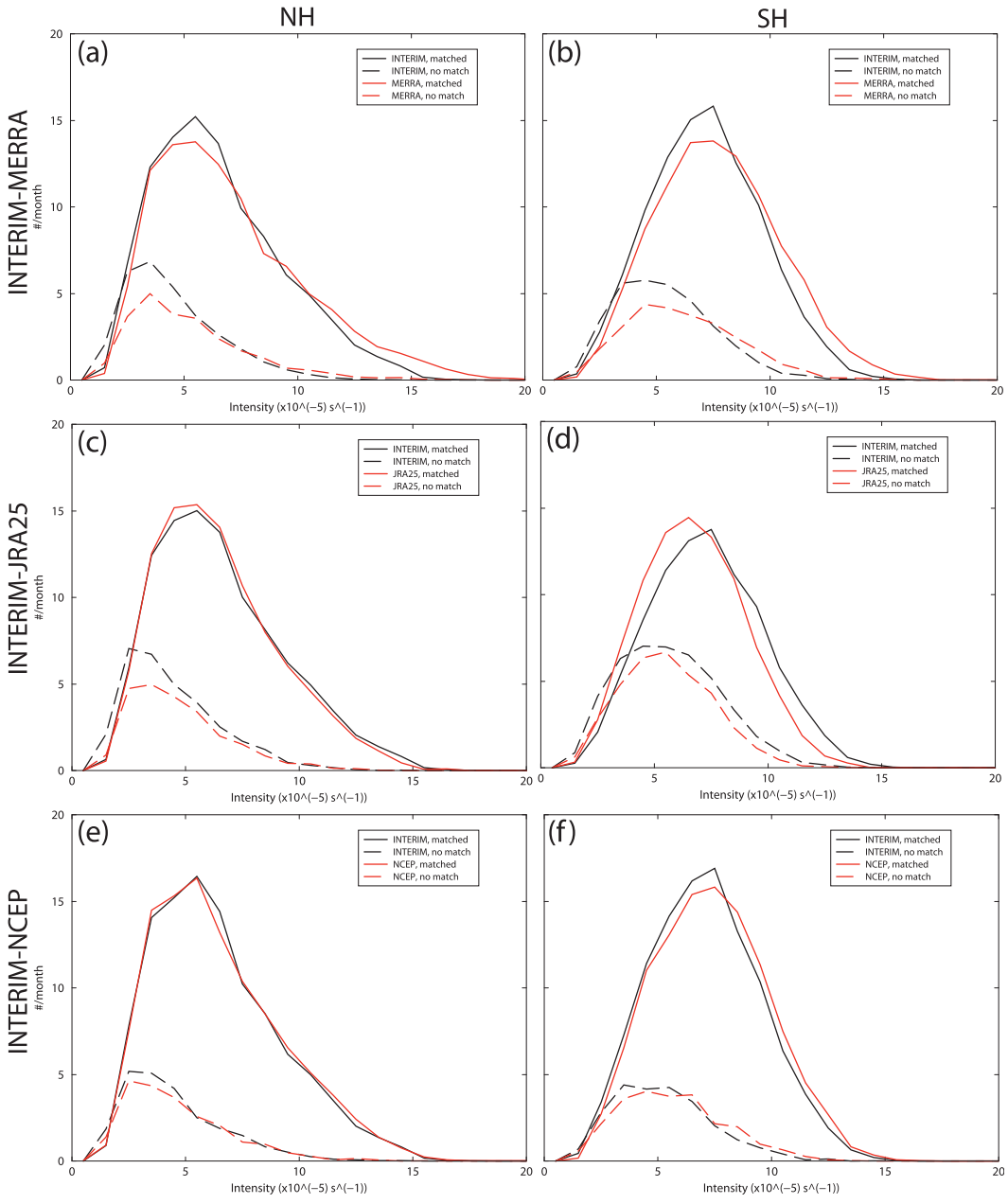


FIG. 5. Maximum intensity distributions for cyclones that match and those that do not match based on the T42 $\xi_{850}$ intensities for Interim − MERRA in (a) the NH and (b) in the SH; Interim − JRA-25 in (c) the NH and (d) the SH; and Interim − NCEP in (e) the NH and (f) the SH. Bin width is $1.0 \times 10^{-5}$ $s^{-1}$.

between JRA-25 and the other reanalyses has a fairly broad distribution compared with the NH, indicating a larger uncertainty in location between the cyclones in JRA-25 and the other reanalyses: this is similar to previous results (Hodges et al. 2004; Wang et al. 2006). However, for the comparison between the newer reanalyses, Fig. 6b shows that there is a significant improvement over the older reanalyses with the mean separation distances generally as good as in the NH, the smallest values occurring for the ERA-Interim comparison with NCEP CFSR. This improvement between the newer reanalyses indicates a reduction in the uncertainty in location that is consistent with the results shown for the track density differences in section 3b.

The instantaneous intensity differences for matched tracks are shown in Fig. 7 for MSLP, 925-hPa winds, and $\xi_{850}$. This diagnostic is useful for indicating both the bias and uncertainty in the intensities, and the location of the

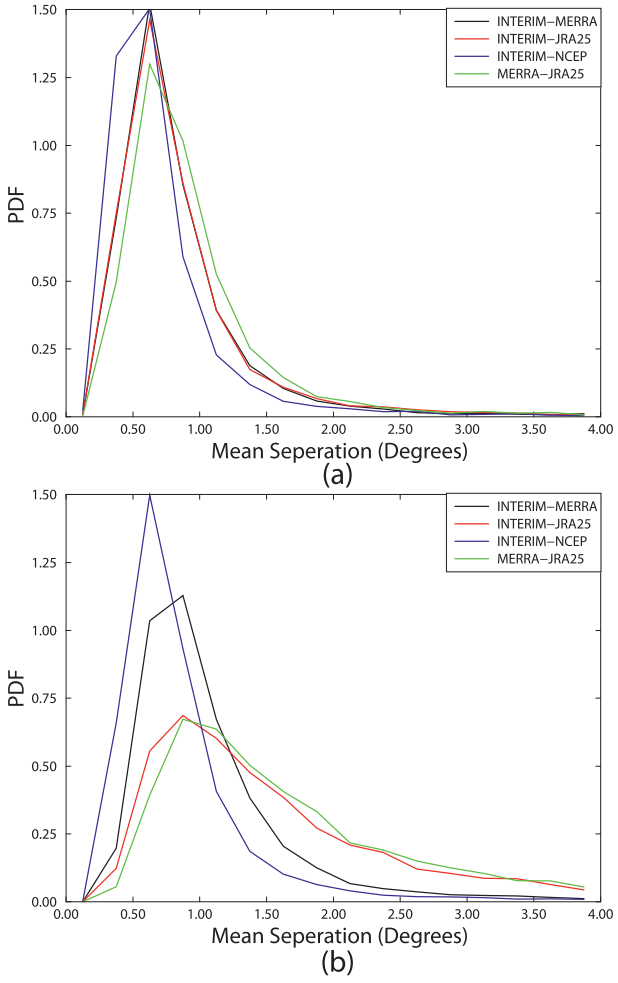


FIG. 6. Probability density distributions for mean separation distance for $\xi_{850}$ tracks that match for (a) the NH and (b) the SH. Units are geodesic degrees, and bin widths are 0.25°.

mode or mean indicates the bias and the breadth of the distribution of the uncertainty. All matched points along the tracks are used. The distributions of differences for MSLP referenced to MSLP tracks are shown in Figs. 7a and 7b for the NH and SH winters, respectively. In the NH the distributions are fairly narrow, indicating that differences between the reanalyses are relatively small. The location of the distributions are centered close to zero for all comparisons except those with NASA MERRA, again highlighting NASA MERRA as having deeper cyclones than the other reanalyses. In the SH the distributions are broader in nature than in the NH, highlighting a greater uncertainty in the intensities. The NCEP CFSR comparison with ERA-Interim still shows a distribution centered on zero and narrower than the other distributions, highlighting the greater similarity between these two reanalyses. NASA MERRA still shows the deepest cyclones and JRA-25 the shallowest. These results are consistent with the maximum intensity distributions shown in section 3c.

For the 925-hPa winds (Figs. 7c and 7d) the distributions indicate fairly similar distributions in the NH and SH for the same compared reanalyses, although the SH distributions are slightly broader. JRA-25 consistently shows the weakest extreme winds compared with the other reanalyses, although it appears more similar to ERA-Interim in the NH than with the other reanalyses. In general, these results are consistent with the results shown in Fig. 4. For the $\xi_{850}$ intensity difference distributions (Figs. 7e and 7f), the results are similar to those for winds except that the distributions are much broader, indicating the larger uncertainty at the smaller spatial scales represented by vorticity. The distributions are also broader in the SH than in the NH though biases are similar between the two hemispheres. These results are consistent with those for the maximum intensity distributions shown in Fig. 4.

### e. *Composite life cycles and structure*

In this section the matching analyses are extended to cyclone life cycles and structure. This is done by identifying a set of intense cyclones in the ERA-Interim reanalysis and then finding the identically same systems in the other reanalyses using the matching methodology as used in the previous section. This is done for both NH and SH winters. The selected cyclones are then used to construct composite life cycles based on the MSLP, 925-hPa winds, and $\xi_{850}$, as discussed in Bengtsson et al. (2009), and horizontal composites of MSLP and system relative winds, as discussed in Catto et al. (2010). The 100 most extreme cyclones are selected in ERA-Interim in each hemisphere in the same way as discussed in Bengtsson et al. (2009), based on the T42 $\xi_{850}$ and with lifetimes longer than 4 days.

Since the composite life cycles generally reflect the intensity results already discussed, they are only briefly discussed and not shown. In the NH winter there is very little difference between the life cycles of the composite cyclones with very similar deepening rates greater than 1 hPa $h^{-1}$. The deepest composite life cycle occurs for NASA MERRA and the shallowest for JRA-25, consistent with the results discussed above. In the SH winter the composite life cyles are deeper than in the NH, related to the circumpolar pressure trough, with growth rates greater than 1 hPa $h^{-1}$, as in the NH. The composite life cycles using 925-hPa winds are also very similar in shape for the different reanalyses, but indicate that the NASA MERRA has a more intense life cycle with respect to the winds and JRA-25 has the weakest life cycle; ERA-Interim and NCEP CFSR have very similar life cycles. This is true for both NH and SH

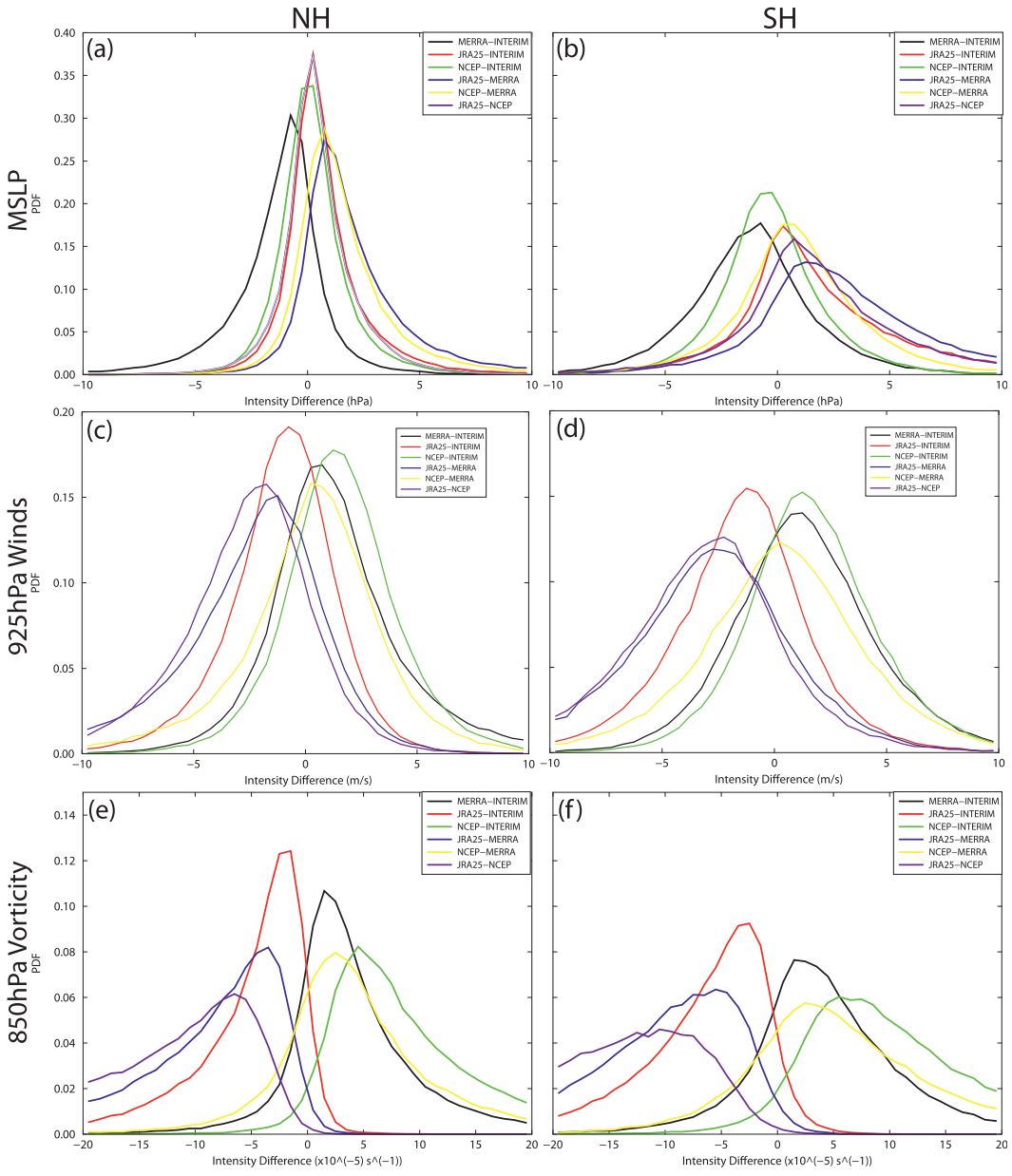


FIG. 7. Probability density distributions for instantaneous intensity differences for the tracks that match: MSLP (hPa), referenced to MSLP tracks with bin widths of 0.5 hPa, in (a) the NH and (b) the SH; 925-hPa winds (m $s^{-1}$), with bin widths of 0.5 m $s^{-1}$, in (c) the NH and (d) the SH; and $\xi_{850}$ ($\times 10^{-5}$ $s^{-1}$), $\xi_{850}$ tracks, bin widths of 1.0 $\times$ $10^{-5}$ $s^{-1}$, in (e) the NH and (f) the SH.

winters. For the $\xi_{850}$ life cycles, again the shapes are very similar but there are larger differences between the intensities, consistent with the maximum intensity distributions shown previously.

The horizontal composites are computed in the same way as described in Bengtsson et al. (2009) and Catto et al. (2010). The method is based on sampling the fields on a radial grid centered on the storm centers with the grid preferred direction rotated to the propagation direction of the storms. This results in the sampled fields appearing to be relative to the storms all moving in the same direction, making storm structural characteristics easier to be identified. The stage of the life cycle at which the composites are produced is chosen as the maximum intensity in the T42, $\xi_{850}$, although any stage can be chosen. A more detailed view of storm structure can be obtained, including the vertical structure, as has previously been performed by Catto et al. (2010); here, only a limited view

is presented based on the MSLP and 925-hPa winds. For the winds, the system relative winds are determined before compositing by subtracting the system velocities.

The horizontal composite results for the NH winter are shown in Fig. 8 with the direction of the composite storm indicated by the large arrow (left to right). This shows that, at least in terms of the variables used here, the structure of the composite cyclones are remarkably similar, particularly for the same features of conceptual models such as discussed by Catto et al. (2010). This includes the general structure of the MSLP field with an extension to the upper right, which possibly indicates the presence of a parent low; this was also discussed by Wang and Rogers (2001). The depth of the composite MSLP cyclones are consistent with the results discussed in previous sections with NASA MERRA having a deeper composite when compared with the other reanalyses. The system relative winds show structures that are very similar between the reanalyses, with relatively weak winds to the right of the direction of motion and a flow orthogonal to the direction in the bottom right quadrant associated with the warm sector flow. The strongest winds occur to the left of the storm direction, with a flow of air rearward relative to the storm motion, which turns cyclonically around the storm center; this is different from earth relative winds, which generally occur behind and to the right of the direction of motion (Catto et al. (2010). These wind structures are similar to those previously discussed by Catto et al. (2010). The intensities of the system relative winds are consistent with the previously discussed results, with NASA MERRA having the larger values. The results for the SH winter are shown in Fig. 9, which shows the same features as those for the NH, albeit the intensities in terms of the depth of the composite cyclone and the system relative winds appear weaker than in the NH. In particular, the warm sector flow in the top right quadrant appears weaker than in the NH composites. The differences between the high-resolution reanalyses also appear weaker but with JRA-25 showing the shallower depth and weaker winds, consistent with the previously discussed results.

In general the results for the composites are consistent with the results discussed in the previous sections in that there is a good agreement between the reanalyses in both hemispheres but with JRA-25, while showing the same life cycle and structure, being weaker than for the other reanalyses, particularly in the SH and with NASA MERRA being the strongest.

## 4. Summary and conclusions

Comparisons have been made between cyclones identified in four recent reanalyses, with the focus being on synoptic scale cyclones, with the aim of determining how well cyclones compare between the reanalyses and any improvements over older reanalyses. A summary of the results are outlined below.

(i) The numbers and spatial distribution of extratropical cyclones compare well in the new high-resolution reanalyses and better than with the lower-resolution JRA-25 reanalysis. This is particularly the case in the NH and also in the SH where the comparison between ERA-Interim and NCEP CFSR is comparable with the NH. This is an improvement over the comparison of the older reanalyses. The largest differences are seen for cyclogenesis in the vicinity of orography, though this improves in the newer reanalyses.

(ii) Greater differences occur between the reanalyses in terms of their maximum intensities, with NASA MERRA having more extreme cyclones in terms of MSLP and winds. For vorticity the intensities are more closely related to the resolution of the models, with NCEP CFSR having the larger intensities. JRA-25 consistently has the weakest intensities for all variables. Differences between the reanalyses become progressively more pronounced, proceeding from MSLP to winds to vorticity.

(iii) Comparing cyclones between the reanalyses using matching shows significant improvements over the older reanalyses with greater than 80% matches in the NH. The systems that do not match tend to be the weaker storms. For the 10% most intense storms the number of matches increases to greater than 97%. The SH shows the most significant improvement over the older reanalyses with the number of matches for the newest reanalyses being almost as good as in the NH—the comparison of ERA-Interim with NCEP CFSR being the best. The number of matched storms are much less for JRA-25 in the SH, similar to the older reanalyses.

(iv) Using the matched storms to explore the uncertainties in the mean separation distances and instantaneous intensity differences indicates that in the NH, all four reanalyses have matches with mean separation distances predominately less than 2° (geodesic), with the lowest mean separation distances occurring for the ERA-Interim comparison with NCEP CFSR. In the SH the comparison of JRA-25 with the other reanalyses shows results similar to the older reanalyses, with a much broader distribution of separation distances than in the NH. However, for the new reanalyses in the SH the separation distances are comparable with the NH—the ERA-Interim comparison with NCEP CFSR being the

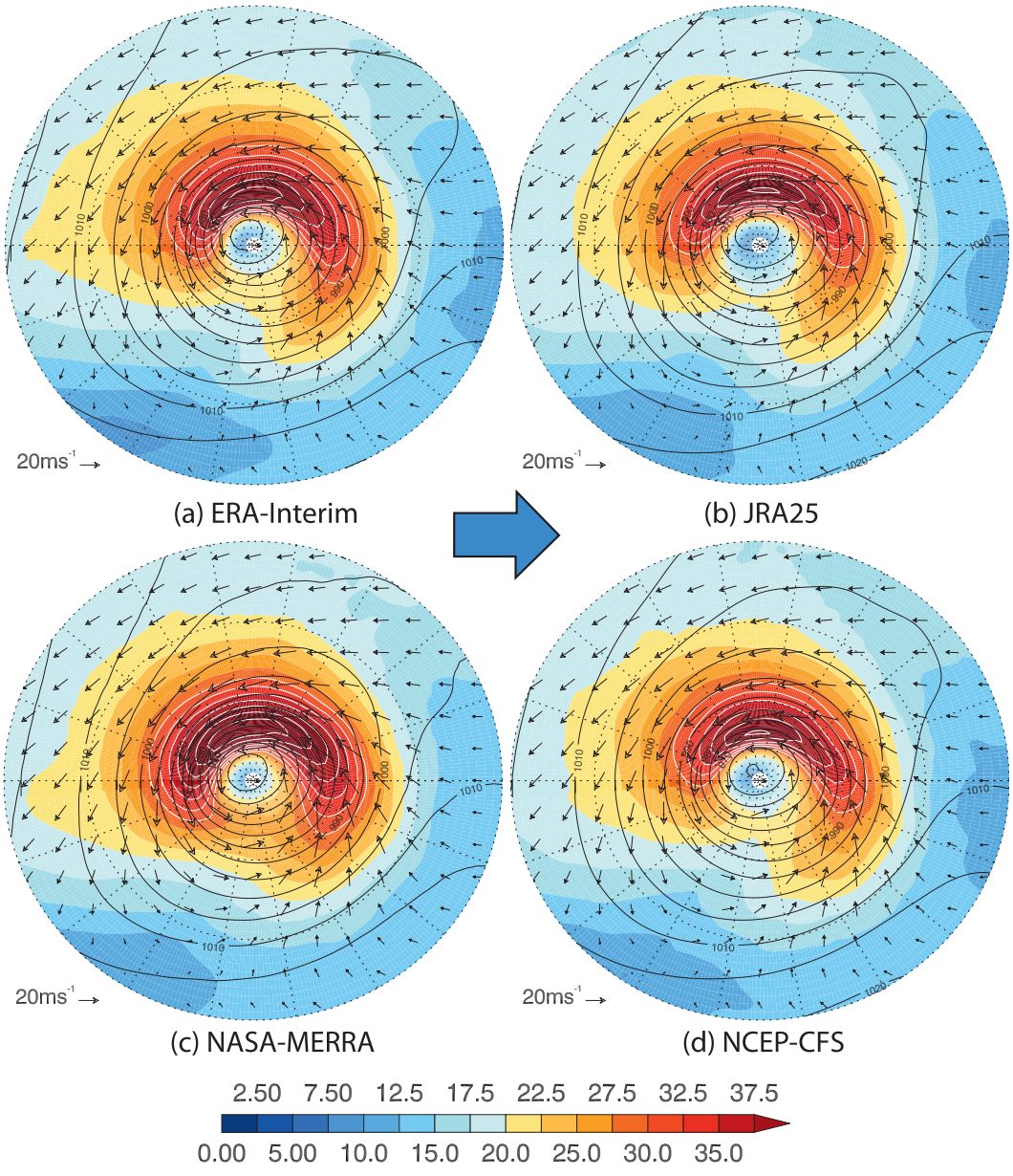


FIG. 8. Horizontal composites of the 100 most intense cyclones identified in ERA-Interim and matched to the other reanalyses of MSLP and system relative winds at 925 hPa for the NH: (a) ERA-Interim, (b) JRA-25, (c) NASA MERRA, and (d) NCEP CFSR. Color contours with interval 2.5 m $s^{-1}$ show the system relative wind speeds with the white lines indicating the highest values starting at 30 m $s^{-1}$, vectors show the system relative wind vectors, and black contours show the MSLP with contour interval 5 hPa. The large blue arrow indicates the direction of the composite storm.

best. The instantaneous intensity bias results are consistent with the maximum intensity distributions, the uncertainty (spread) increases proceeding from pressure to winds to vorticity.

(v) The composite cyclones indicate that for the different reanalyses these are very similar, with the main differences reflecting the intensity differences seen in the intensity distribution statistics. Similar structures to those discussed by Catto et al. (2010) are found.

The results have shown that there is considerable improvement in the agreement between the new high-resolution reanalyses compared with older reanalyses or with the lower resolution JRA-25 reanalyses. This is consistent with the improvement in models, observations, and

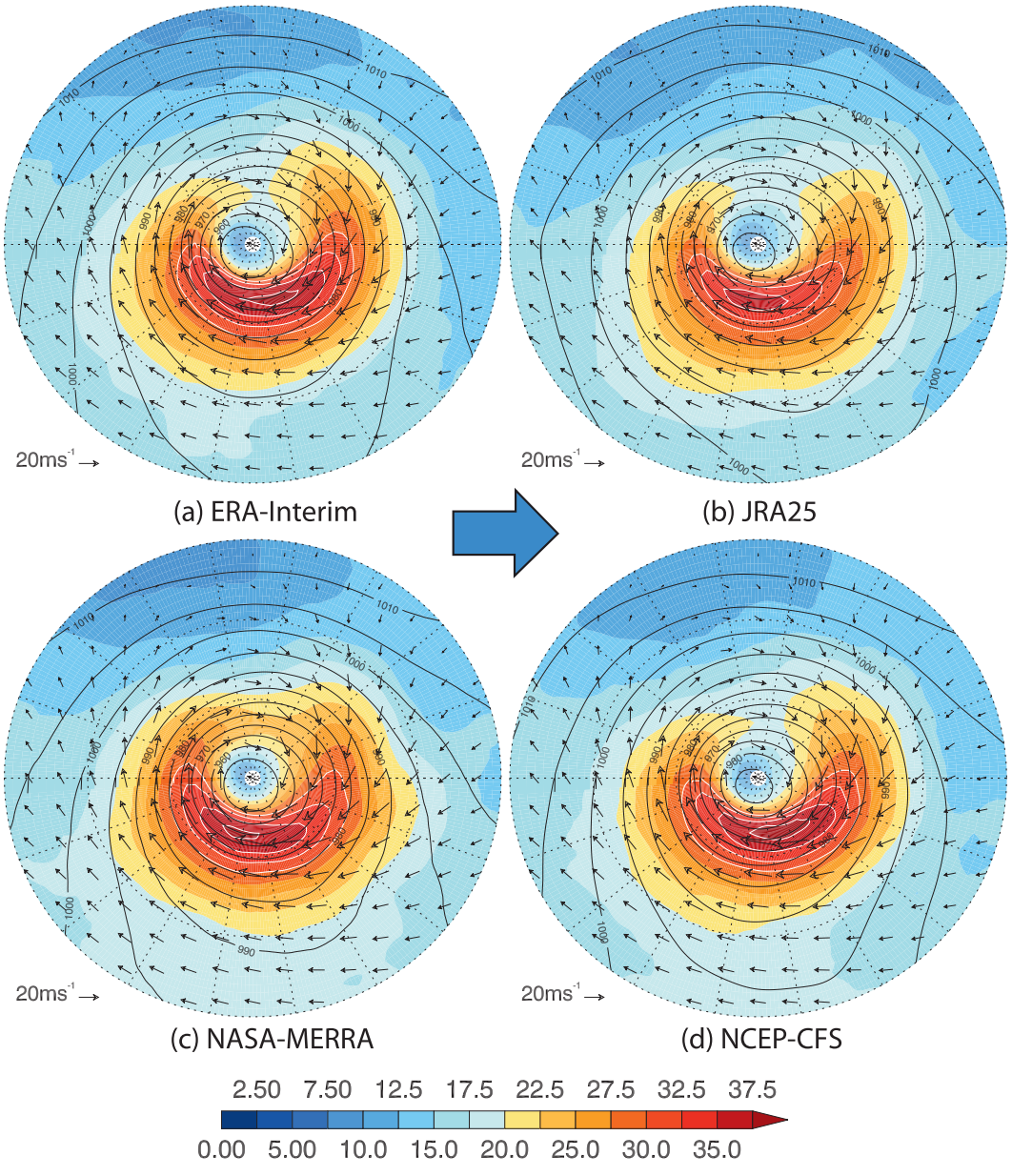


FIG. 9. As in Fig. 8 but for the SH.

data assimilation in NWP systems, such that predictive skill is now as good in the SH as in the NH. It is in the vicinity of orography that large differences in the cyclogenesis are seen, which improves considerably for the newer high-resolution reanalyses, though problems still persist in the vicinity of the high but narrow Andes. One spatial difference seen between the older reanalyses that persists with the newer reanalyses occurs at the end of the Mediterranean storm track in both track density and cyclogenesis though this reduces in the newer reanalyses, in particular for the ERA-Interim comparison with NCEP CFSR. This is likely due to the fact that these storms are relatively weak and more dependent on the forecast model, observations, and data assimilation methods. The fact that the weaker systems agree less well between the reanalyses is also apparent in the track matching analysis.

One of the big improvements in assimilating observations has been the direct assimilation of satellite radiances; this was shown to have an impact on the older reanalyses (Bromwich et al. 2007). However, there were still larger differences in the SH, where satellite data dominates, than in the NH. This might suggest that the satellite observations solely are insufficient to constrain the whole of the troposphere. However, for the

new high-resolution reanalyses, the differences in the SH are comparable with those in the NH indicating that more information is being extracted from the available observations by the new data assimilation methods supplemented by new observations, such as scatterometer winds and improved microwave sounder observations.

Perhaps the most surprising results occur for the intensities, particularly that of the larger number of extremes in NASA MERRA for MSLP and winds compared with the other reanalyses. It is difficult to explain why NASA MERRA should have more and larger extremes of pressure and winds than the other reanalyses, but the fact that the storms are deeper is likely to lead to stronger geostrophic winds. The intensity in terms of vorticity is perhaps more clearly understandable, as it is closely linked to the resolution of the different reanalysis systems with the small spatial scales represented by the vorticity being more sensitive to resolution.

The matching results further confirm the agreement between the new high-resolution reanalyses, such that in the NH the cyclones compare to a high degree, both in terms of numbers and location, with the systems that do not match tending to be the weakest ones; this is also true for the lower resolution JRA-25 in the NH. The biggest improvement in agreement occurs in the SH where comparisons between the high-resolution reanalyses are almost as good as in the NH. The composite analysis of the matched storms further highlights the similarity of cyclones between the reanalysis, in particular for the structure. There is much scope to extend the composite analysis to the full 3D structure and to verify the cyclone properties directly against observations, particularly from satellites (Field et al. 2008; Naud et al. 2010).

While the focus of the study has been on the ERA-Interim period (1989–2009), using the longer periods from 1979 of the other reanalyses gives similar results, with only a small degradation in results for the earlier periods.

We have intercompared the different reanalyses and showed that there is an improvement in their agreement with respect to extratropical cyclones, particularly in the SH, compared with the older reanalyses. The convergence of the newer high-resolution reanalyses provides some confidence that the reanalyses are representing these storms at least equally well. However, it does not tell us that extratropical cyclones are being correctly represented in every respect, as differences are still apparent for the intensities of storms and it is not possible to tell from a simple intercomparison which one is closest to reality. This has to be done by comparing directly with observations, ideally independent from the assimilated observations. However, this is made difficult by the inhomogeneous nature of the observations. This in part can be reconciled by using the available satellite observations, which provide much better coverage than terrestrial observations. This is an area of current work. Future work will also focus on a similar comparison for mesocyclones and tropical cyclones.

*Acknowledgments.* The authors would like to acknowledge the Global Modeling and Assimilation Office (GMAO) and the GES DISC for the dissemination of the MERRA data. The JRA-25 data was produced and supplied by the Japan Meteorological Agency (JMA) and the Central Research Institute of Electric Power Industry (CRIEPI). The ERA-Interim data has been produced by ECMWF and obtained as part of a member state special project. The CFSR data were developed by NOAA's National Centers for Environmental Prediction (NCEP). The data for this study are from the NOAA Operational Model Archive and Distribution System (NOMADS), which is maintained at the NOAA National Climatic Data Center (NCDC).

## REFERENCES

Anderson, D., K. I. Hodges, and B. J. Hoskins, 2003: Sensitivity of feature-based analysis methods of storm tracks to the form of background field removal. *Mon. Wea. Rev.,* **131,** 565–573.

Andersson, E., and H. Järvinen, 1999: Variational quality control. *Quart. J. Roy. Meteor. Soc.,* **125,** 697–722.

Bengtsson, L., K. I. Hodges, and S. Hagemann, 2004: Sensitivity of large-scale atmospheric analyses to humidity observations and its impact on the global water cycle and tropical and extratropical weather systems in ERA40. *Tellus,* **56A,** 202–217.

——, ——, and E. Roeckner, 2006: Storm tracks and climate change. *J. Climate,* **19,** 3518–3543.

——, and Coauthors, 2007: The need for a dynamical climate reanalysis. *Bull. Amer. Meteor. Soc.,* **88,** 495–501.

——, K. I. Hodges, and N. Keenlyside, 2009: Will extratropical storms intensify in a warmer climate? *J. Climate,* **22,** 2276–2301.

Bromwich, D. H., R. L. Fogt, K. I. Hodges, and J. E. Walsh, 2007: A tropospheric assessment of the ERA-40, NCEP, and JRA-25 global reanalyses in the polar regions. *J. Geophys. Res.,* **112,** D10111, doi:10.1029/2006JD007859.

Catto, J. L., L. C. Shaffrey, and K. I. Hodges, 2010: Can climate models capture the structure of extratropical cyclones? *J. Climate,* **23,** 1621–1635.

Chang, E. K. M., 1993: Downstream development of baroclinic waves as inferred from regression analysis. *J. Atmos. Sci.,* **50,** 2038–2053.

Field, P. R., A. Gettelman, R. Neale, R. Wood, P. J. Rasch, and H. Morrison, 2008: Midlatitude cyclone compositing to constrain climate model behavior using satellite observations. *J. Climate,* **21,** 5887–5903.

Froude, L. S. R., 2010: TIGGE: Comparison of the prediction of Northern Hemisphere extratropical cyclones by different ensemble prediction systems. *Wea. Forecasting,* **25,** 819–836.

Gibson, J. K., P. Kållberg, S. Uppala, A. Nomura, A. Hernandez, and E. Serrano, 1997: ERA description. ECMWF Re-Analysis Final Report Series 1, 71 pp.

Griffies, S., M. J. Harrison, R. C. Pacanowski, and A. Rosati, 2004: A technical guide to MOM4. GFDL Ocean Group Tech. Rep. 5, NOAA/Geophysical Fluid Dynamics Laboratory, 342 pp.

Hanson, C., J. Palutikof, and T. Davies, 2004: Objective cyclone climatologies of the North Atlantic—A comparison between the ECMWF and NCEP reanalyses. *Climate Dyn.,* **22,** 757–769.

Hodges, K. I., 1994: A general method for tracking analysis and its application to meteorological data. *Mon. Wea. Rev.,* **122,** 2573–2586.

——, 1995: Feature tracking on the unit sphere. *Mon. Wea. Rev.,* **123,** 3458–3465.

——, 1996: Spherical nonparametric estimators applied to the UGAMP model integration for AMIP. *Mon. Wea. Rev.,* **124,** 2914–2932.

——, 1999: Adaptive constraints for feature tracking. *Mon. Wea. Rev.,* **127,** 1362–1373.

——, 2008: Confidence intervals and significance tests for spherical data derived from feature tracking. *Mon. Wea. Rev.,* **136,** 1758–1777.

——, B. J. Hoskins, J. Boyle, and C. Thorncroft, 2003: A comparison of recent reanalysis datasets using objective feature tracking: Storm tracks and tropical easterly waves. *Mon. Wea. Rev.,* **131,** 2012–2037.

——, ——, ——, and ——, 2004: Corrigendum. *Mon. Wea. Rev.,* **132,** 1325–1327.

Hólm, E., E. Andersson, A. Beljaars, P. Lopez, J.-F. Mahfouf, A. J. Simmons, and J. N. Thépaut, 2002: Assimilation and modeling of the hydrological cycle: ECMWF's status and plans. ECMWF Tech. Memo. 383, 55 pp.

Hoskins, B. J., and K. I. Hodges, 2002: New perspectives on the Northern Hemisphere winter storm tracks. *J. Atmos. Sci.,* **59,** 1041–1061.

——, and ——, 2005: New perspectives on the Southern Hemisphere storm tracks. *J. Climate,* **18,** 4108–4129.

Kalnay, E., 2003: *Atmospheric Modeling, Data Assimilation, and Predictability*. Cambridge University Press, 341 pp.

Lin, S. J., 2004: A vertically Lagrangian finite-volume dynamical core for global models. *Mon. Wea. Rev.,* **132,** 2293–2307.

Naud, C., A. D. Del Genio, M. Bauer, and W. Kovari, 2010: Cloud vertical distribution across warm and cold fronts in *CloudSat*–CALIPSO data and a general circulation model. *J. Climate,* **23,** 3397–3415.

Onogi, K., and Coauthors, 2007: The JRA-25 Reanalysis. *J. Meteor. Soc. Japan,* **85,** 369–432.

Purser, R. J., W.-S. Wu, D. F. Parrish, and N. M. Roberts, 2003a: Numerical aspects of the application of recursive filters to variational statistical analysis. Part I: Spatially homogeneous and isotropic Gaussian covariances. *Mon. Wea. Rev.,* **131,** 1524–1535.

——, ——, ——, and ——, 2003b: Numerical aspects of the application of recursive filters to variational statistical analysis. Part II: Spatially inhomogeneous and anisotropic general covariances. *Mon. Wea. Rev.,* **131,** 1536–1548.

Rančić, M., J. C. Derber, D. Parrish, R. Treadon, and D. T. Kleist, 2008: The development of the first-order time extrapolation to the observation (FOTO) method and its application in the NCEP global data assimilation system. *Proc. 12th Conf. IOAS-AOLS,* New Orleans, LA, Amer. Meteor. Soc., 6.1. [Available online at http://ams.confex.com/ams/88Annual/techprogram/paper_131816.htm.]

Rienecker, M. M., and Coauthors, 2008: The GEOS-5 Data Assimilation System—Documentation of versions 5.0.1 and 5.1.0. NASA GSFC Tech. Rep. Series on Global Modeling and Data Assimilation, NASA/TM-2007-104606, Vol. 27, 92 pp.

——, and Coauthors, 2011: MERRA: NASA's Modern-Era Retrospective Analysis for Research and Applications. *J. Climate,* **24,** 3624–3648.

Saha, S., and Coauthors, 2006: The NCEP Climate Forecast System. *J. Climate,* **19,** 3483–3517.

——, and Coauthors, 2010: The NCEP Climate Forecast System reanalyses. *Bull. Amer. Meteor. Soc.,* **91,** 1015–1057.

Schubert, S. D., R. B. Rood, and J. Pfaendtner, 1993: An assimilated dataset for earth science applications. *Bull. Amer. Meteor. Soc.,* **74,** 2331–2342.

Simmons, A., S. Uppala, D. Dee, and S. Kobayashi, 2007: ERA-Interim: New ECMWF reanalysis products from 1989 onwards. *ECMWF Newsletter,* No. 110, ECMWF, Reading, United Kingdom, 25–35.

Thépaut, J.-N., and E. Andersson, 2003: Assimilation of high-resolution satellite data. *ECMWF Newsletter,* No. 97, ECMWF, Reading, United Kingdom, 6–12.

——, R. Hoffman, and P. Courtier, 1993: Interactions of dynamics and observations in a four-dimensional variational assimilation. *Mon. Wea. Rev.,* **121,** 3393–3414.

Trigo, I. F., 2006: Climatology and interannual variability of storm-tracks in the Euro-Atlantic sector: A comparison between ERA-40 and NCEP/NCAR reanalyses. *Climate Dyn.,* **26,** 127–143.

Uppala, S. M., and Coauthors, 2005: The ERA-40 Re-Analysis. *Quart. J. Roy. Meteor. Soc.,* **131,** 2961–3012.

Wang, C.-C., and J. C. Rogers, 2001: A composite study of explosive cyclogenesis in different sectors of the North Atlantic. Part I: Cyclone structure and evolution. *Mon. Wea. Rev.,* **129,** 1481–1499.

Wang, X. L., V. R. Swail, and F. W. Zwiers, 2006: Climatology and changes of extratropical cyclone activity: Comparison of ERA-40 with NCEP–NCAR reanalysis for 1958–2001. *J. Climate,* **19,** 3145–3166.

Wu, W.-S., R. J. Purser, and D. F. Parrish, 2002: Three-dimensional variational analysis with spatially inhomogeneous covariances. *Mon. Wea. Rev.,* **130,** 2905–2916.